Dalton Transactions

ROYAL SOCIETY OF CHEMISTRY

PAPER

View Article Online
View Journal | View Issue

Cite this: *Dalton Trans.*, 2023, **52**, 1357

Salen, salan and salalen zinc(II) complexes in the interaction with HS^-: time-resolved fluorescence applications†

Maria Strianese, *[a] Gerard Joseph D'Auria,[a] Marina Lamberti,[a] Alessandro Landi,[a] Andrea Peluso,[a] Antonio Varriale,[b,c] Sabato D'Auria[d] and Claudio Pellecchia[a]

Received 19th November 2022,
Accepted 3rd January 2023

DOI: 10.1039/d2dt03730k

rsc.li/dalton

In the current work we investigate the route of interaction of a newly synthesized family of zinc complexes with HS^- by a plethora of different spectroscopic techniques. A computational analysis on the time dependent density functional theory (TD-DFT) level explored the overall fluorescence properties of the title complexes and their different fluorescence responses to HS^-. Time-resolved fluorescence experiments were also performed and highlight the great potential of the current systems to be implemented as HS^- fluorescent sensors.

Introduction

In the last decades, along with its traditional toxic role, hydrogen sulfide (H_2S) emerged for its beneficial functions for humans, depending on the concentration.[1–3] This was a consequence of the discovery that it occurs naturally in the human body[4,5] with diverse roles in cardioprotection,[6] neuroprotection,[7] wound healing,[8,9] and mitigating oxidative stress and associated damage.[2,10,11]

Various diseases such as Huntington's disease, asthma, and Crohn's disease seem to be associated with decreased H_2S levels,[12–16] and establishing whether the downregulation of H_2S production is one of the contributing causes or one of the symptoms of these diseases is still a challenging question. And overall the mechanisms by which H_2S exerts its biological reactivity are not completely clear yet.[17] One molecular mechanism that has been proposed for H_2S as a beneficial bio-molecule is the posttranslational modification of protein cysteine residues forming persulfide (RSSH):[18–20] this process has been called "sulfhydration" or persulfhydration. This reaction generates S^0 that seems involved in several aspects of H_2S chemistry, and that has the high potential of transducing signals owing to its unique property of transsulfuration.

From a different point of view, the mechanisms of action of H_2S can be envisioned to involve interactions with transition metals and, in this context, the study of its coordination chemistry appears highly interesting. Motivated by our interest in shedding light on the biochemical reactions H_2S is involved in, our studies on the coordination of H_2S to transition metals started some time ago and focused both on properly tailored low molecular weight compounds and on natural metalloproteins.[21–30] More recently we focused on zinc salen-based complexes and targeted these systems as efficient scaffolds for isolating and characterizing hydrosulfido species and as performing HS^- sensing constructs *via* a 'coordinative-based' mechanism.[31–36] We and others also reported that the fluorescence of ZnSalen complexes can be fine-tuned by an *ad-hoc* design of the ligands' electronic states[37] and that is both dependent on the electronic states of the diamine moiety bridging the two nitrogens which chelate the zinc center and on the substituents on the salycilaldehyde units.[35,38] In addition, we showed that the electronic state of the diamine moiety between the zinc-chelating nitrogens strongly modulates the photophysical properties of the salen complexes so as their fluorescence response to hydrogen sulfide.[31,35] Starting from these achievements, in the current work, we decided to explore whether the imine functionalities of the salen complexes play a determining role in the interaction of the sensor molecule and HS^-. In other words since, as well acknowledged in the literature, *salen* stands for *N*,*N*′-bis(salicylidene)ethylenediamine and refers to a tetradentate *C*2-symmetric ligand with both sp^2-hybridized nitrogen atoms synthesized from salycilalde-

[a]*Dipartimento di Chimica e Biologia "Adolfo Zambelli", Università degli Studi di Salerno, Via Giovanni Paolo II, 132, 84084 Fisciano (SA), Italy.*
E-mail: mstriane@unisa.it
[b]*Institute of Food Science, CNR Italy, 83100 Avellino, Italy*
[c]*URT-ISA, CNR at Department of Biology, University of Naples Federico II, 80126 Napoli, Italy*
[d]*Department of Biology, Agriculture, and Food Sciences, National Research Council of Italy (CNR-DISBA), Piazzale Aldo Moro 7, 00185 Rome, Italy*
†Electronic supplementary information (ESI) available. See DOI: https://doi.org/10.1039/d2dt03730k

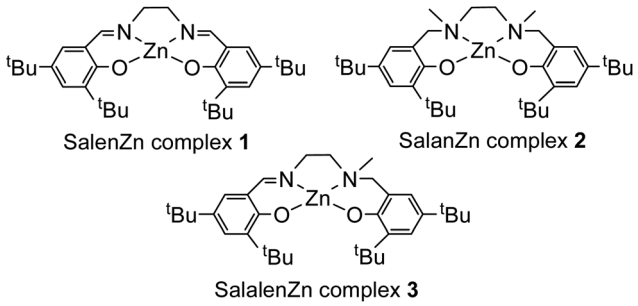

Scheme 1

hyde (sal) and ethylenediamine (en); we thought of exploring the tetrahydro derivative of *salen*, named *salan* (which displays two phenoxyamine functionalities and a sp^3 hybridization of the amine nitrogen atoms) together with the *salalen* (which is the dihydro derivative of *salen* and is also considered a hybrid derivative of *salen*/*salan* ligands with sp^2- and sp^3-hybridized nitrogen atoms).[39,40] and of comparing the reactivity of the related complexes with HS^-. We synthesized a new family of zinc complexes derived from *salen*, *salan* and *salalen* ligands with the same substituents on the salycilaldehyde units (Scheme 1) and investigated the possible effects of these ligands on the zinc hydrosulfido stabilization. We also wanted to answer the question whether the different ligand structures would tune the fluorescence properties of the related complexes as HS^- sensors: the different hybridization of the nitrogen atoms in these classes of tetradentate ligands may differentiate the behaviour of the corresponding complexes in a substantial way.

Results and discussion

Complexes **1–3** were synthesized by the direct reaction of the ligand precursors and $ZnEt_2$ in dry benzene and were first characterized *via* high-resolution MALDI Fourier transform ion cyclotron resonance mass spectrometry (HR MALDI-FT-ICR) (Fig. S1–S3†). The major peaks at 555.291 *m*/*z* units for complex **1**, at 586.346 *m*/*z* units for complex **2** and at 570.314 *m*/*z* units for complex **3** correspond to the mononuclear species: no evidence for binuclear species in solution were found. In a second instance, complexes were characterized *via* ^{1}H NMR experiments (Fig. S4–S7†). The ^{1}H NMR spectra of complexes **1–3** in DMSO-d_6 exhibit sharp signals consistent with the expected coordination of the ligand. For complex **1** the solubility in deuterated dimethylsulfoxide was scarce, therefore the ^{1}H NMR spectrum is not well resolved (Fig. S4†) whereas it resulted completely soluble in deuterated methylene chloride: the protonic spectrum of complex **1** in CD_2Cl_2 is displayed in Fig. S5.† The spectra of complexes **2** and **3** in DMSO-d_6 are reported in Fig. S6 and S7.† The presence of AB patterns for the methylenic protons of the ethylene bridge and/or for the methylenic protons between the coordinating nitrogen and the aromatic moiety, highlights the coordination of the nitrogen atoms to the zinc centers in each complex. Furthermore, comparison of the ^{1}H NMR spectra of the free ligands (Fig. S8–S10†) with those of the related complexes points to similar conclusions: by overlapping the spectrum of each ligand with that of the complex a shift of most of the signals is visible; in addition the spectra of the ligands exhibit signals at *circa* 11 ppm ascribable to the O***H*** of the phenolates (missing in the spectra of the complexes) together with the equivalence of the methylenic protons of the ethylene bridge (Fig. S8–S10†).

After characterization of complexes **1–3** we started a study to establish the mechanism of their interaction with HS^-. To assess which is the operating route of interaction, we first examined the reactions *via* high-resolution MALDI-FT-ICR. Fig. S11–S13† display the outcome of our experiments. As for complex **1** and complex **3**, binding of the HS^- seems the working reaction route (Fig. S11 and S13†): the major peaks at 587.267 and at 603.296 *m*/*z* units are consistent with the mononuclear [complex **1**/HS]$^-$ and [complex **3**/HS]$^-$ species. MS experiments clearly indicate the formation of 1 : 1 HS^- adducts for complexes **1** and **3**.

Differently for complex **2** mass experiments suggest displacement of the zinc from the organic ligand (Fig. S12†): the peak at 523.425 *m*/*z* units exhibits the isotopic pattern of the salan ligand and the peak at 545.40 corresponds to the [salan ligand + Na]$^+$ (Fig. S12†). Most likely, the different behavior of complex **2** respect to complexes **1** and **3** maybe due to the fact that the presence of the amine backbone results in a more flexible structure.

Aiming at further insights on the mechanism of the reaction between the title complexes and HS^-, we analyzed the protonic NMR spectra of complexes **1–3** in the presence of NaSH. Fig. 1 displays the ^{1}H NMR spectrum of complex **3** in the presence of HS^-.

In the presence of an excess of NaSH, the whole pattern of signals of complex **3** undergoes a shift (Fig. 1 and also Fig. S14†). In addition, in the spectrum of the complex **3**/HS adduct (see Fig. 1), the high field signal (at ∼−2.7 ppm) which, as well acknowledged in the literature,[27,30–33,35,41–43] indicates binding of SH^- to the zinc center, is also present.

The hypothesis of HS^- coordination to the zinc center could be drawn also when analyzing the ^{1}H NMR spectrum of complex **1** in the presence of NaSH (Fig. S17†). Differently, in case of complex **2** the protonic spectrum in the presence of NaSH points to leaching of the organic ligand (Fig. S9 *vs.* S15 and S16†). The resulting spectrum is not well resolved, most likely for the concomitant precipitation of ZnS occurring; furthermore, peaks ascribable to the free ligand are also evident (Fig. S16†). Hence, the NMR experiments corroborate the results of the MS experiments.

Next, we tested the optical properties of complexes **1–3** to assess their potential use in the recognition of HS^-. Fig. 2 displays the UV-vis spectra of the title complexes before and after the treatment with an excess of HS^-.

As evident in Fig. 2, for all the complexes under investigation the interaction with HS^- results in a change of the

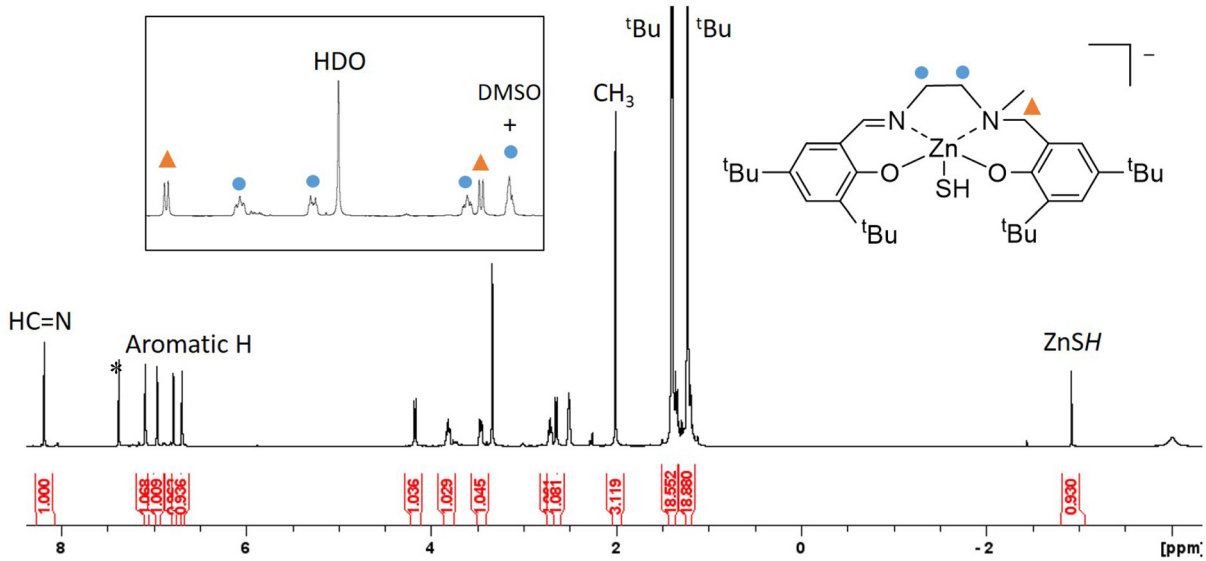

Fig. 1 ^{1}H NMR spectrum of complex **3** in DMSO-d_6 after the addition of an excess of HS^-. [Complex **3**] = 5 × 10^{-3} M; [NaSH] = 0.01 M. * = benzene used for the synthesis.

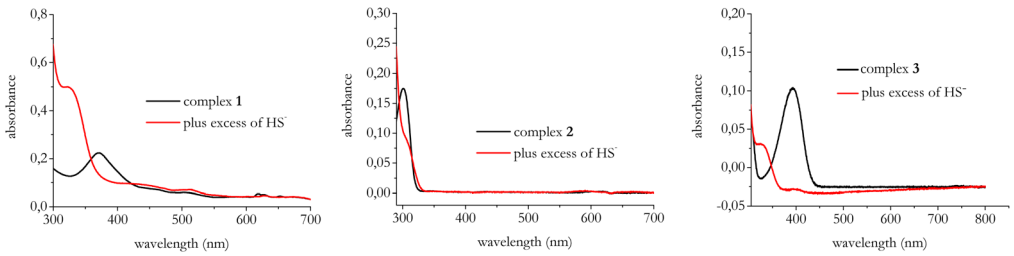

Fig. 2 Electronic absorption spectra of complexes **1–3** with and without the addition of 50 μM of NaSH. Spectra were recorded in DMSO at room temperature. [Complexes] = 10 μM.

initial UV-visible spectrum which points to the formation of new species.

Then, we studied the fluorescence responses of the title complexes to HS^-. Fig. 3 displays the results of the steady-state fluorescence experiments.

In the presence of HS^- the fluorescence responses indicate visible quenching effects for complexes **1** and **2** whereas complex **3** undergoes to fluorescence enhancement.

As for complex **2**, we also checked the fluorescence of ligand **2** which resulted very weak (see Fig. S17†), most likely as a consequence of its reduced coniugation, thus the fluorescence quenching observed in the presence of HS^- further strengthens that displacement of the zinc from the organic ligand takes place upon interaction with HS^-.

Willing to rationalize these experimental results and above all to understand why complexes **1** and **3** exhibit a different

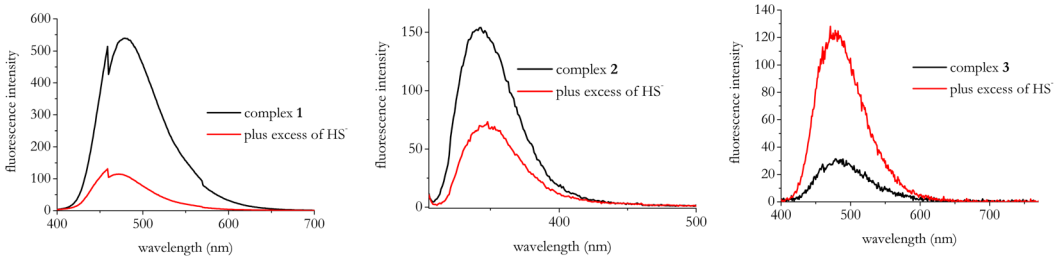

Fig. 3 Emission spectra of complexes **1–3** before and after the addition of 5 equiv. of NaSH. [Complexes **1–3**] = 1 × 10^{-5} M; [NaSH] = 5 × 10^{-5} M. All spectra were measured in DMSO with λ_{exc} = 370 nm for complex **1**; λ_{exc} = 300 nm for complex **2**; λ_{exc} = 300 nm for complex **3**.

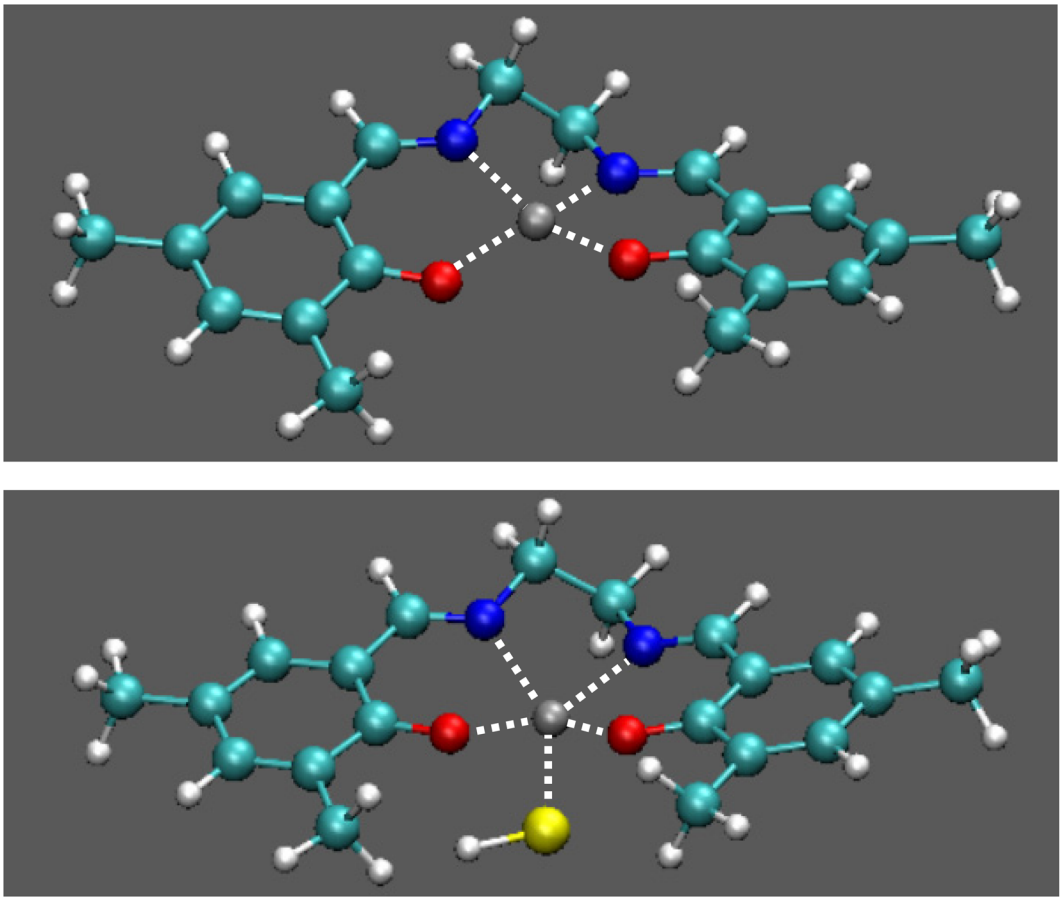

Fig. 4 Optimized geometries for complex **1** (top) and its adduct with HS^-.

fluorescence response to HS^- while MS and NMR experiments indicate HS^- binding to the zinc centers in both cases, we performed a computational analysis at the time dependent density functional theory (TD-DFT) level. Minimum energy geometries of complex **1** and complex **3** and of their HS^- adducts (also considering the possibility of multiple adducts) have been computed both for the ground state and for the first excited singlet states. The computed ground state optimum geometries of **1** and of its HS^- complex are shown in Fig. 4 (a similar geometry has been also found for **3** and its HS^- adduct, Fig. S19†).

Complex **1** and **3** deviate from the square planar nuclear configuration observed for more rigid analogues,[31,35] with the metal atom in the plane of the ligand, see Fig. 4 and Fig. S19.† The formation of the single adduct is predicted to be exoergonic (ΔE = −0.65 eV for complex **1**, ΔE = −0.70 eV for complex **3**), whereas the double adducts are not predicted to be stable species, as confirmed by DFT computation where the second HS^- is moved away from the metal centre during geometry optimization. This finding is also in line with the MS experiments (Fig. S11 and S13†).

Emission from S_1 is predicted to be electric dipole allowed both for **1** and **3** and for their HS^- adducts. Computed vertical and adiabatic excitation energies are reported in Table 1, together with the oscillator strengths for the $S_1 \leftarrow S_0$ transitions.

Table 1 Computed vertical and adiabatic excitation energies (eV) and oscillator strength for the $S_1 \leftarrow S_0$ transitions

	Vertical	Adiabatic	Oscillator strength
1	3.71	3.02	0.19
1 + HS^-	3.64	2.92	0.20
3	3.75	3.00	0.20
3 + HS^-	3.62	2.93	0.23

For **1** two electric dipole transition are predicted at around 334 and 321 nm; since they are very close, they are not distinguished in the experimental spectra, which shows only one peak, whereas in the case of **3** the prediction points to one peak at 340 nm, as in the experimental trace (Fig. 2).

However, a meaningful comparison between predicted and observed absorption spectra would require a band shape simulations, with the computations of Franck–Condon integrals[44,45] which is far beyond the qualitative purposes of the present computational analysis.

Since for all the species emission from S_1 are electric dipole allowed transitions, the different behaviour observed for **1** and **3** and for their HS^- complexes has to be related with the

possible existence of non-radiative decay paths. We have thus investigated the energy location of the lowest triplet states, which could be responsible of the different fluorescence quantum yields of **1** and **3** and their HS^- adducts (see Table S1†).

The energies of the four lowest triplet states are reported in Fig. 5; T_5 lies always above in energy than S_1 and therefore it should not be involved in non-radiative decay paths. T_2 and T_1 are significantly lower in energy than S_1 for all the species and therefore, based on the energy gap rule, the direct transition $S_1 \rightarrow T_1$ and $S_1 \rightarrow T_2$ should not be an efficient decay path. The triplet states closer in energy to S_1 are T_3 and T_4.

As concerns complex **1**, T_3 and T_4 are almost isoenergetic, both before and after HS^- coordination, thus offering a double channel for non-radiative decay from S_1. Moreover, these exoergonic $S_1 \rightarrow T_3$ and $S_1 \rightarrow T_4$ transition are more favoured after HS^- coordination, as demonstrated by the lower energy difference between the electronic states and by the higher spin–orbit coupling for $S_1 \rightarrow T_3$. Thus, a strong quenching of fluorescence is to be expected in presence of HS^-, as indeed observed (Fig. 3).

On the contrary, the $S_1 \rightarrow T_4$ transition is exoergonic for **3**, but it becomes slightly endoergonic (−50 meV) when the HS^- is coordinated (Fig. 5). Together with the lowering of the spin orbit coupling element (Table 2), this suggests that quenching of fluorescence *via* S1 → T4 is possible in the isolated complex, whereas fluorescence is recovered in presence of HS^- in solution, in line with experimental observations (Fig. 3).

Time-resolved fluorescence experiments

To further explore the sensing abilities of complexes **3** and **1** (the complexes of this family working *via* the coordinative-based approach) we studied their responses to HS^- by means of time-resolved fluorescence spectroscopy.[46] The results for complex **3** show an increase of the average lifetime in the presence of NaSH in the sample solution from 2.51 to 4.08 ns (see also Table S2 and Fig. S20 in the ESI†).

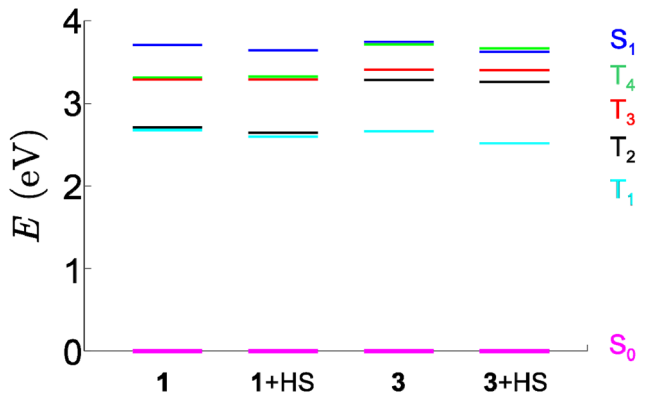

Fig. 5 Computed energies (*E*, eV) of the ground state (S_0) first excited singlet (S_1), and four lowest energy triplet states, evaluated at the S_1 geometry for complex **1** and **3**, and their HS^- adducts.

Table 2 Spin–orbit coupling elements (cm^{-1}) for **1**, **3** and their adducts

	SOC T3-S1	SOC T4-S1
1	1.16473	28.86538
1 + HS^-	18.17608	12.30915
3	2.69732	6.60415
3 + HS^-	1.27732	1.33585

As proposed in previous work this finding is in line with the enhancement of the fluorescence intensity observed in the steady-state measurements: when probe-analyst interaction results in fluorescence enhancement the increases of the corresponding lifetime is generally found in most cases.[47,48]

Indeed, when on the contrary there is a fluorescence quenching upon coordination of HS^- to the complex, such as in complex **1**, we observe a reduction of the average lifetime (from 5.08 to 3.36 ns) upon addition of the NaSH in the sample solution (see Table S3 and Fig. S21 in the ESI†).

Time-resolved fluorescence spectroscopy has been extensively used by some of us for applications in biological contexts thus ensuring a broad applicability of this technology in the field of (bio)sensing.[46,49,50]

H_2S sensing applications

In the following experiments we focused on complex **3** which was the only one of the series undergoing a fluorescence enhancement in the presence of HS^- and thus useful for practical sensing measurements (*e.g.* "turn on" systems are inherently more sensitive than "turn-off" sensors).

First, we checked whether we could construct a calibration of the system by monitoring the change of its initial fluorescence intensity after the addition of increasing concentrations of NaSH. Fig. 6A shows the response of the fluorescence switching of complex **3** for a series of subsequent measurements with increased concentrations of NaSH. Fig. 6B displays the fluorescence intensity values at 480 nm fit against HS^- concentration.

From Fig. 6 it results that the detection limit of the system is in the micromolar range of H_2S.

We also explored the selectivity of complex **3** in the recognition of HS^- against biologically relevant and potentially competing thiols (*e.g.* glutathione (GSH) and L-cysteine (L-cys)). In the presence of both GSH and L-cys we observed a quenching of the initial fluorescence emission of complex **3** (Fig. 7) thus pointing to selectivity of the system towards HS^- recognition.

As for the time-resolved fluorescence experiments, we observed very modest responses in the average lifetimes from 2.1 to 2.75 ns in the presence of GSH and from 1.98 to 2.19 ns in case of L-Cys, again pointing to selectivity of complex **3** in HS^- recognition (see Fig. S22, S23, Tables S4 and S5†).

In a second instance we studied the time response of complex **3** by monitoring its fluorescence intensity as a function of time upon HS^- addition. Fig. 8 displays a typical time

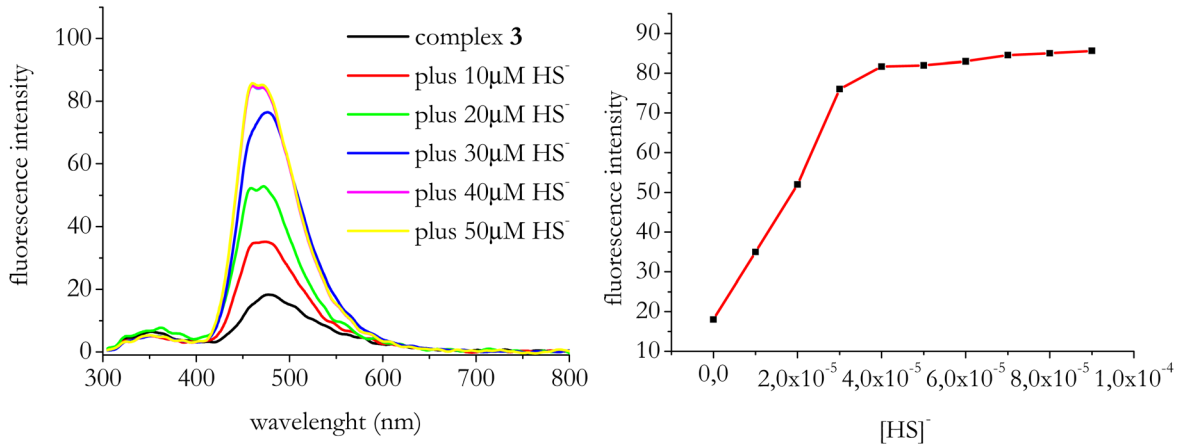

Fig. 6 Left: emission spectra of complex **3** (λ_{exc} = 300 nm) when titrated with NaSH. [Complex **3**] = 1 × 10^{-5} M; end concentration of NaSH varied in the range (1–5) × 10^{-5} M. Right: fit of the fluorescence intensity values of complex **3** at 480 nm against HS^- concentration.

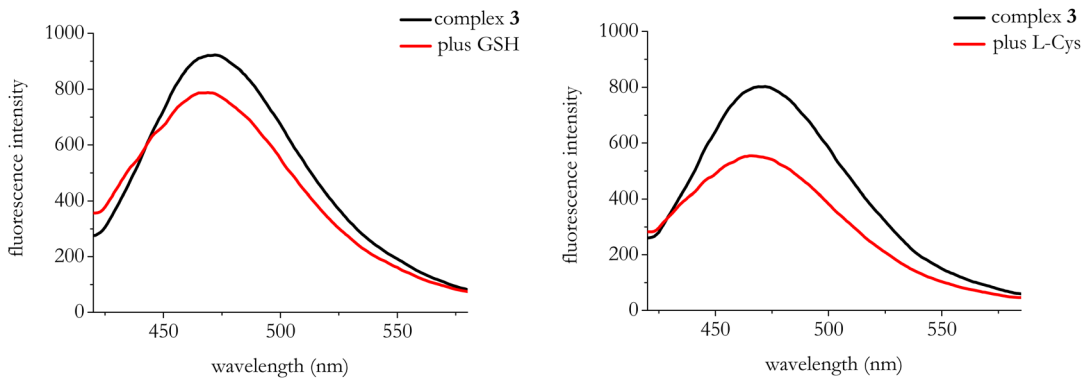

Fig. 7 Emission spectra of complex **3** (λ_{exc} = 300 nm) in the presence of GSH and L-Cys. GSH = 50 mM; L-Cys = 50 mM.

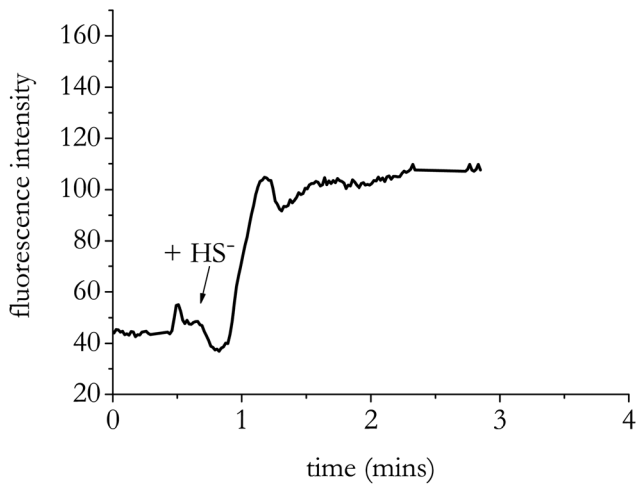

Fig. 8 Fluorescence intensity time trace observed at 480 nm (exc 300 nm) of complex **3**, upon addition of HS^-.

trace of a solution containing 10 μM of complex **3** when excited at 300 nm.

Conclusions

In conclusion, in the framework of our ongoing studies aiming at shedding light on the coordination chemistry of HS^- to bio-inorganic targets, and in particular to salen-type zinc complexes, we synthesized and characterized a new family of salen-derived zinc complexes and investigated their reactivity with HS^-. By means of different spectroscopic techniques, we assessed coordination of HS^- to the zinc center for complex **1** and complex **3** whereas for complex **2** our experiments point to precipitation of ZnS and leaching of the organic ligand. This difference may be due to the different 'hardness/softness' of imine and amine nitrogens which chelate the zinc centers: the 'soft' imine nitrogens in complex **1** may coordinate the metal

center more strongly than the harder amine nitrogens in complex **2**.

Steady-state fluorescence experiments assessed that the fluorescence intensity of the complexes is modulated by the presence of HS^- and the different responses have been rationalized by means of a computational analysis. The different fluorescence trends observed for **1** and **3** in the presence of HS^- has been related with the possible existence of non-radiative decay paths.

Preliminary time-resolved fluorescence experiments provided evidences that the current systems experience consistent differences in the average lifetimes in response to HS^-, more precisely in the presence of NaSH complex **3** shows an increase of the average lifetime from 2.51 to 4.08 ns conversely complex **1** exhibits a reduction from 5.08 to 3.36 ns. These results are in line with the steady-state fluorescence measurements.

To the best of our knowledge, this is one of the first studies in which zinc compounds are used for sensing HS^- by means of time-resolved fluorescence spectroscopy and we do believe that this study could open the doors to new kind of applications for practical measurements in the fast growing field of H_2S monitoring.

Experimental section

Materials

Chemicals used for the synthetic work were obtained from Sigma-Aldrich or Strem Chemicals and were of reagent grade. They were used without further purification. NaSH (Alfa Aesar) in aqueous solution was used as HS^- source to the end concentration specified in the figure captions. Syntheses of ligands were performed by following literature procedures.[40,51–53] Syntheses of complexes **1** and **2** were achieved by modifications of literature procedures.[54,55]

General

HR MALDI and ESI mass spectra were recorded using a Bruker solariX XR Fourier transform ion cyclotron resonance (FT-ICR) mass spectrometer (Bruker Daltonik GmbH, Bremen, Germany) equipped with a 7 T refrigerated actively-shielded superconducting magnet (Bruker Biospin, Wissembourg, France). The samples were ionized in positive ion mode using either the MALDI ion or the ESI ion source. The mass range was set to *m*/*z* 150–2000. The laser power was 15% and 15 laser shots were used for each scan. Mass spectra were calibrated externally using a mix of peptide clusters in MALDI ionization positive ion mode. As for the ESI mass spectra, they were calibrated externally using a NaTFA solution in negative ion mode. A linear calibration was applied.

NMR spectra were recorded on a Bruker AVANCE 400 NMR instrument (^{1}H NMR, 400.13 MHz; ^{13}C NMR, 100.62 MHz) or on a 600 MHz spectrometer [600 (^{1}H NMR) and 150 MHz (^{13}C NMR)] using 5 mm o.d. NMR tubes. The chemical shifts were reported in δ (ppm) referenced to SiMe4. Typically, 5 mg of the complex in 0.5 mL of the solvent were used for each experiment. MilliQ water and is the water filtered with a Millipore filter apparatus.

Characterization of complex 1. MS (MALDI FT-ICR MeOH): *m*/*z* (%) calculated: 555.292 experimental: 555.291 [complex **1** + H]$^+$. ^{1}H NMR [400 MHz, CD_2Cl_2]: δ = 7.91 (s, 2H, C***H***=N), 7.42 (d, *J* = 2.36 Hz, 2H, Ar***H***), 6.6 (d, *J* = 2.36 Hz, 2H, Ar***H***), 4.08 (d, *J* = 12.39 Hz, 2H, N-C***H***H-C***H***H-N), 3.77 (d, *J* = 12.39 Hz, 2H, N-C***H***H-C***H***H-N), 1.41 (s, 18H, ^{t}***Bu***), 1.27 (s, 18H, ^{t}***Bu***). Emission (DMSO, λ_{exc} = 370 nm), λ_{max}, nm (quantum yield, Φ_F): 478 nm (0.4).

Characterization of complex 2. MS (MALDI FT-ICR MeOH): *m*/*z* (%) calculated: 586.347 experimental: 586.346 [complex **2**]$^+$. ^{1}H NMR [300 MHz, DMSO-d_6]: δ = 7.02 (d, *J* = 2.43 Hz, 2H, Ar***H***), 6.70 (d, *J* = 2.43 Hz, 2H, Ar***H***), 7.20 (s, 1H, Ar***H***), 3.60 (s, 4H, N-C***H***$_2$-Ar), 2.81 (d, *J* = 9.30 Hz, 2H, N-C***H***H-C***H***H-N), 2.29 (d, *J* = 9.30 Hz, 2H, N-CH***H***-CH***H***-N), 2.09 (s, 6H, C***H***$_3$), 1.34 (s, 18H, ^{t}***Bu***), 1.19 (s, 18H, ^{t}***Bu***).

Characterization of complex 3. MS (MALDI FT-ICR MeOH): *m*/*z* (%) calculated: 570.315 experimental: 570.314 [complex **3**]$^+$. ^{1}H NMR [300 MHz, DMSO-d_6]: δ = 8.39 (s, 1H, C***H***=N), 7.2 (s, 1H, Ar***H***), 6.99 (s, 1H, Ar***H***), 6.89 (s, 1H, Ar***H***), 6.71 (s, 1H, Ar***H***), 3.99 (d, *J* = 11.60 Hz, 1H, N-C***H***H-Ar), 3.65 (bs, 2H, N-C***H***$_2$-CH$_2$-N), 3.04 (d, *J* = 11.60 Hz, 1H, N-C***H***H-Ar), 2.66 (bs, 2H, N-CH$_2$-C***H***$_2$-N), 2.15 (s, 3H, C***H***$_3$), 1.44 (d, 9H, ^{t}***Bu***), 1.37 (s, 9H, ^{t}***Bu***), 1.23 (s, 9H, ^{t}***Bu***), 1.21 (s, 9H, ^{t}***Bu***). Emission (DMSO, λ_{exc} = 300 nm), λ_{max}, nm (quantum yield, Φ_F): 483 nm (0.06).

Absorbance and fluorescence measurements. Absorption spectra were recorded on a Cary-50 Spectrophotometer, using a 1 cm quartz cuvette (Hellma Benelux bv, Rijswijk, Netherlands) and a slit-width equivalent to a bandwidth of 5 nm. Fluorescence spectra were measured on a Cary Eclipse Spectrophotometer in a 10 × 10 mm^2 airtight quartz fluorescence cuvette (Hellma Benelux bv, Rijswijk, Netherlands) with an emission band-pass of 10 nm and an excitation band-pass of 5 nm. Both absorption and fluorescence measurements were performed in DMSO solutions at 25 °C. Fluorescence emission spectra were registered by exciting the samples at a specific wavelength (as stated in the figure captions).

Fluorescence quantum yield (Φ_F) values were measured in optically diluted solutions using as standards the commercial dye Cy3 NHS (Φ_F = 0.15 in MilliQ water), according to the equation:[46]

$$\Phi_F{}^s = \Phi_F{}^r (I_s/I_r)(A_r/A_s)(\eta_s/\eta_r)^2$$

where indexes *s* and *r* denote the sample and reference, respectively. *I* stands for the integrated emission intensity, *A* is the absorbance at the excitation wavelength, and η is the refractive index of the solvent. The optical density of complexes **1** and **3** and standards was kept below 0.1. The uncertainty in the determination of Φ_F is ±15%.

NMR characterization of the complexes 1–3 upon addition of HS^-. The NMR tube was charged with the free complex solutions in DMSO-d_6 then NaSH solid or in solution (to the end

concentrations specified in the figure captions) was added and the spectra registered.

Computational details. All electronic computations have been carried out at the density functional level of theory using the range separated hybrid functional CAM-B3LYP with TZVP basis set as implemented in the Gaussian package (G09).[56] That combination of functional and basis set has been chosen because it leads to accurate predictions, as discussed in previous work.[57] Time dependent DFT (TD-DFT) has been employed for treating all excited states. Spin–orbit coupling elements have been computed by PySOC code.[58] In order to reduce the computational cost, solvent molecules have not been considered explicitly in the computations; instead, effects due to solvent (DMSO) polarization were included in the computations by the polarizable continuum model (PCM),[59] which has been shown to lead to molecular properties in good agreement with experiments.[44,60,61]

Lifetime measurements. Frequency-domain lifetime measurements were performed by frequency domain methods using Chronos (ISS inc. Illinois, USA) fluorescence lifetime spectrometer. For complex **3**, measurements were performed using a light-emitting diodes (LED) at 300 nm. The sample prepared in dimethyl sulfoxide (DMSO) and optical densities, measured on Jasco V-550 UV/Vis spectrophotometer (Jasco, Japan), were 0.1 O.D. at the excitation wavelength. A similar procedure was used for the sample preparation of complex **1** but the lifetime measurements were performed using a laser diode at 370 nm as excitation source, and signals were collected at the magic angle of 54.7° to eliminate possible contribution from fluorescence anisotropy decay. In both cases, the measurements were carried out at room temperature.

The intensity decays were analyzed with Vinci software using the multi-exponential model:

$$I(t) = \sum \alpha_i \exp(-t/\tau_i)$$

where $I(t)$ is the intensity at a time τ, α_i is the amplitude of the ith component, and τ_i is the lifetime of the ith component.

The average decay lifetime is defined as:

$$\langle \tau \rangle_i = \sum \alpha_i \tau_i / \sum \alpha_i$$

The acceptability of the fits was estimated by χ^2 and the mean (average) fluorescence lifetimes were calculated.

Conflicts of interest

There are no conflicts to declare.

References

1 K. Abe and H. Kimura, *J. Neurosci.*, 1996, **16**, 1066.
2 J. L. Wallace and R. Wang, *Nat. Rev. Drug Discovery*, 2015, **14**, 329–345.
3 G. Yang, L. Wu, B. Jiang, W. Yang, J. Qi, K. Cao, Q. Meng, A. K. Mustafa, W. Mu, S. Zhang, S. H. Snyder and R. Wang, *Science*, 2008, **322**, 587.
4 W. Xuan, C. Sheng, Y. Cao, W. He and W. Wang, *Angew. Chem., Int. Ed.*, 2012, **51**, 2282–2284.
5 C. Q. Chen, H. Xin and Y. Z. Zhu, *Acta Pharmacol. Sin.*, 2007, **28**, 1709–1716.
6 M. Lavu, S. Bhushan and D. Lefer, *Clin. Sci.*, 2010, **120**, 219–229.
7 W. L. Chen, Y. Y. Niu, W. Z. Jiang, H. L. Tang, C. Zhang, Q. M. Xia and X. Q. Tang, *Rev. Neurosci.*, 2015, **26**, 129–142.
8 M. Xu, Y. Hua, Y. Qi, G. Meng and S. Yang, *Exp. Dermatol.*, 2019, **28**, 776–785.
9 H. Zhao, S. Lu, J. Chai, Y. Zhang, X. Ma, J. Chen, Q. Guan, M. Wan and Y. Liu, *J. Diabetes Complicat.*, 2017, **31**, 1363–1369.
10 S. Carballal, M. Trujillo, E. Cuevasanta, S. Bartesaghi, M. a. N. Möller, L. K. Folkes, M. A. Garcìa-Bereguiaìn, C. Gutiérrez-Merino, P. Wardman, A. Denicola, R. Radi and B. Alvarez, *Free Radical Biol. Med.*, 2011, **50**, 196–205.
11 C. M. Levinn and M. D. Pluth, *Sens. Actuators, B*, 2021, **329**, 129235.
12 M. Whiteman, S. Le-áTrionnaire, M. Chopra, B. Fox and J. Whatmore, *Clin. Sci.*, 2011, **121**, 459–488.
13 S. B. Singh and H. C. Lin, *Microrganisms*, 2015, **3**(4), 866–889.
14 P. Wang, G. Zhang, T. Wondimu, B. Ross and R. Wang, *Exp. Physiol.*, 2011, **96**, 847–852.
15 K. F. Chung, *Expert Rev. Respir. Med.*, 2014, **8**, 5–13.
16 K. G. Fosnacht, M. D. Hammers, M. S. Earp, A. K. Gilbert and M. D. Pluth, *Chem. – Asian J.*, 2022, **17**(16), DOI: **10.1002/asia.2022200426**.
17 Q. Li and J. R. Lancaster, *Nitric Oxide*, 2013, **35**, 21–34.
18 A. K. Mustafa, M. M. Gadalla, N. Sen, S. Kim, W. Mu, S. K. Gazi, R. K. Barrow, G. Yang, R. Wang and S. H. Snyder, *Sci. Signaling*, 2009, **2**, ra72, DOI: **10.1126/scisignal.2000464**.
19 B. D. Paul and S. H. Snyder, *Nat. Rev. Mol. Cell Biol.*, 2012, **13**, 499–507.
20 N. Sen and S. H. Snyder, *Trends Neurosci.*, 2010, **2010/09/16**, 493–502.
21 S. Mirra, S. Milione, M. Strianese and C. Pellecchia, *Eur. J. Inorg. Chem.*, 2015, 2272–2276.
22 M. Strianese, A. Varriale, M. Staiano, C. Pellecchia and S. D'Auria, *Nanoscale*, 2011, **3**(1), 298–302.
23 M. Strianese, S. Milione, V. Bertolasi, C. Pellecchia and A. Grassi, *Inorg. Chem.*, 2011, **50**, 900–910.
24 M. Strianese, F. De Martino, C. Pellecchia, G. Ruggiero and S. D'Auria, *Protein Pept. Lett.*, 2011, **18**, 282–286.
25 M. Strianese, G. J. Palm, S. Milione, O. Kuhl, W. Hinrichs and C. Pellecchia, *Inorg. Chem.*, 2012, **51**, 11220–11222.
26 M. Strianese, S. Mirra, V. Bertolasi, S. Milione and C. Pellecchia, *New J. Chem.*, 2015, **39**, 4093–4099.
27 M. Strianese, M. Lamberti and C. Pellecchia, *Dalton Trans.*, 2017, **46**, 1872–1877.

28 M. Strianese, S. Mirra, M. Lamberti and C. Pellecchia, *Inorg. Chim. Acta*, 2017, **466**, 426–431.
29 M. Strianese, G. J. Palm, D. Kohlhause, L. A. Ndamba, L. C. Tabares and C. Pellecchia, *Eur. J. Inorg. Chem.*, 2019, **2019**, 885–891.
30 M. Strianese, S. Brenna, G. Ardizzoia, D. Guarnieri, M. Lamberti, I. D'Auria and C. Pellecchia, *Dalton Trans.*, 2021, **50**, 17075–17085.
31 M. Strianese, V. Vykhovanets, N. Blal, D. Guarnieri, A. Landi, M. Lamberti, A. Peluso and C. Pellecchia, *Sensors*, 2022, **22**, 3173.
32 M. Strianese, M. Lamberti and C. Pellecchia, *Dalton Trans.*, 2018, **47**, 17392–17400.
33 M. Strianese, M. Lamberti, A. Persico and C. Pellecchia, *Inorg. Chim. Acta*, 2019, 119235.
34 M. Strianese and C. Pellecchia, *Coord. Chem. Rev.*, 2016, **318**, 16–28.
35 M. Strianese, D. Guarnieri, M. Lamberti, A. Landi, A. Peluso and C. Pellecchia, *Inorg. Chem.*, 2020, **59**, 15977–15986.
36 M. Strianese, D. Pappalardo, M. Mazzeo, M. Lamberti and C. Pellecchia, *Dalton Trans.*, 2020, **49**, 16533–16550.
37 G. Consiglio, I. P. Oliveri, S. Failla and S. Di Bella, *Molecules*, 2019, **24**, 2514.
38 D. Xie, J. Jing, Y. B. Cai, J. Tang, J. J. Chen and J. L. Zhang, *Chem. Sci.*, 2014, **5**, 2318–2327.
39 S. p. Bellemin-Laponnaz and S. Dagorne, Coordination chemistry and applications of salen, salan and salalen metal complexes, in *Chemistry of Metal Phenolates*, John Wiley Ltd, Chichester, UK, 2014, pp. 263–309.
40 A. Yeori, S. Gendler, S. Groysman, I. Goldberg and M. Kol, *Inorg. Chem. Commun.*, 2004, **7**, 280–282.
41 M. Rombach and H. Vahrenkamp, *Inorg. Chem.*, 2001, **40**, 6144–6150.
42 M. D. Pluth and Z. J. Tonzetich, *Chem. Soc. Rev.*, 2020, **49**, 4070–4134.
43 E. Galardon, A. Tomas, M. Selkti, P. Roussel and I. Artaud, *Inorg. Chem.*, 2009, **48**, 5921–5927.
44 A. Capobianco, R. Borrelli, A. Landi, A. Velardo and A. Peluso, *J. Phys. Chem. A*, 2016, **120**, 5581–5589.
45 A. Landi, R. Borrelli, A. Capobianco, A. Velardo and A. Peluso, *J. Chem. Theory Comput.*, 2018, **14**, 1594–1601.
46 R. Joseph. *Lakowicz Principles of Fluorescence Spectroscopy*, 2006.
47 B. Das, S. Dey, G. P. Maiti, A. Bhattacharjee, A. Dhara and A. Jana, *New J. Chem.*, 2018, **42**, 9424–9435.
48 S. Das, M. Das, S. Laha, K. Rajak, I. Choudhuri, N. Bhattacharyya, B. C. Samanta and T. Maity, *J. Mol. Struct.*, 2022, **1263**, 133214.
49 S. D'Auria, E. Apicella, M. Staiano, S. Di Giovanni, G. Ruggiero, M. Rossi, P. Sarkar, R. Luchowski, I. Gryczynski and Z. Gryczynski, *Anal. Biochem.*, 2012, **425**, 13–17.
50 A. Varriale, V. Marzullo, S. Giovanni, A. Scala, A. Capo, A. Majoli, A. Pennacchio and M. Staiano, *Anal. Bioanal. Chem.*, 2016, **408**, 6329–6336.
51 E. Y. Tshuva, N. Gendeziuk and M. Kol, *Tetrahedron Lett.*, 2001, **42**, 6405–6407.
52 P. Hormnirun, E. L. Marshall, V. C. Gibson, R. I. Pugh and A. J. P. White, *Proc. Natl. Acad. Sci. U. S. A.*, 2006, **103**, 15343–15348.
53 M. Cozzolino, V. Leo, C. Tedesco, M. Mazzeo and M. Lamberti, *Dalton Trans.*, 2018, **47**, 13229–13238.
54 Q. Dong, X. Ma, J. Guo, X. Wei, M. Zhou and D. Liu, *Inorg. Chem. Commun.*, 2008, **11**, 608–611.
55 G. A. Morris, H. Zhou, C. L. Stern and S. T. Nguyen, *Inorg. Chem.*, 2001, **40**, 3222–3227.
56 M. J. Frisch, G. W. Trucks and H. B. Schelegel. et al. *Gaussian 09, revision D.01*, Gaussian, Wallingford, 2009. Ref Type: Computer Program.
57 C. J. Cramer and D. G. Truhlar, *Phys. Chem. Chem. Phys.*, 2009, **11**, 10757–10816.
58 X. Gao, S. Bai, D. Fazzi, T. Niehaus, M. Barbatti and W. Thiel, *J. Chem. Theory Comput.*, 2017, **13**, 515–524.
59 S. Miertus, E. Scrocco and J. Tomasi, *Chem. Phys.*, 1981, **55**, 117–129.
60 A. Capobianco, A. Landi and A. Peluso, *Phys. Chem. Chem. Phys.*, 2017, **19**, 13571–13578.
61 B. Mennucci, J. Tomasi, R. Cammi, J. R. Cheeseman, M. J. Frisch, F. J. Devlin, S. Gabriel and P. J. Stephens, *J. Phys. Chem. A*, 2002, **106**, 6102–6113.